Tidal Modulation of Antarctic Ice Shelf Melting

Ole Richter[1,2], David E. Gwyther[1], Matt A. King[2], and Benjamin K. Galton-Fenzi[3]

[1]Institute for Marine and Antarctic Studies, University of Tasmania, Private Bag 129, Hobart, TAS, 7001, Australia.
[2]Geography & Spatial Sciences, School of Technology, Environments and Design, University of Tasmania, Hobart, TAS, 7001, Australia.
[3]Australian Antarctic Division, Kingston, TAS, 7050, Australia.

Correspondence: Ole Richter (ole.richter@utas.edu.au)

Abstract. Tides influence basal melting of individual Antarctic ice shelves, but their net impact on Antarctic-wide ice-ocean interaction has yet to be constrained. Here we quantify the impact of tides on ice shelf melting and the continental shelf seas by means of a 4 km resolution circum-Antarctic ocean model. Activating tides in the model increases the total basal mass loss by 57 Gt/yr (4 %), while decreasing continental shelf temperatures by 0.04 °C. The Ronne Ice Shelf features the highest increase in mass loss (44 Gt/yr, 128 %), coinciding with strong residual currents and warming temperatures on the adjacent continental shelf. Regional variations can be an order of magnitude larger, with strong melt modulations in buttressing important regions of cold regimes. Further, to explore the processes that cause variations in melting we apply dynamical-thermodynamical decomposition to the melt drivers in the boundary layer. In most regions, tidal current modulation of the turbulent exchange of heat and salt across the ice-ocean boundary layer has a strong contribution. In some regions, however, mechanisms driven by thermodynamic effects are equally or more important, including under the frontal parts of Ronne Ice Shelf. Our results support the importance of capturing tides for robust modelling of glacier systems and shelf seas, and motivate future studies to directly assess friction-based parameterisations for the pan-Antarctic domain.

1 Introduction

Changes in the ocean have been identified to modulate melting at the base of Antarctic ice shelves with consequences for sea-level rise and global climate (e.g. Pritchard et al., 2012; Liu et al., 2015; Bronselaer et al., 2018). The oceanic mechanisms that govern the heat transport across the continental shelf and within sub-ice shelf cavities, however, remain poorly understood and quantified, contributing to large uncertainties in the prediction of future changes (e.g. Asay-Davis et al., 2017; Turner et al., 2017).

One relevant mechanism is ocean tides, as they interact with ice shelves in many ways including ice shelf basal melting (Padman et al., 2018). At the ice base, tidal currents enhance the turbulent exchange of heat and salt through the ice-ocean boundary layer and therefore modulate local melt rates as well as melt water driven buoyant plumes that affect ice-ocean interaction downstream (MacAyeal, 1984; Makinson and Nicholls, 1999). Away from the ice shelf base, friction at the sea bed and underneath static sea ice contributes to ocean mixing (e.g. Padman et al., 2009; Llanillo et al., 2019), as does breaking of internal waves excited by tidally oscillating flow over steep sloping topography (e.g. Padman et al., 2006; Foldvik et al., 1990). Further, tidal currents can be rectified into a mean flow component (Loder, 1980) with velocity magnitudes comparable to the ambient circulation (Padman et al., 2009; MacAyeal, 1985; Makinson and Nicholls, 1999). By means of these mechanisms, tides are thought to play a fundamental role in the heat transport across the continental shelf break (Padman et al., 2009; Stewart et al., 2018), vertical mixing and advection at the ice front (Gammelsrod and Slotsvik, 1981; Foldvik et al., 1985; Makinson and Nicholls, 1999) and upwelling of warm deep water inside sub-ice shelf cavities (MacAyeal, 1984). The roles of these processes for ice shelf-ocean interaction in an Antarctic-wide context, however, are not well understood, inhibiting reliable parameterisations in large scale climate simulations (Asay-Davis et al., 2017; Jourdain et al., 2019).

Regional ocean-ice shelf models that explicitly resolve tides have now been successfully applied to all large ice shelves around Antarctica (e.g. Makinson et al., 2011; Mueller et al., 2012, 2018; Galton-Fenzi et al., 2012; Robertson, 2013; Arzeno et al., 2014; Mack et al., 2017; Jourdain et al., 2019). The combined domains, however, do not cover all of the Antarctic coastline, neglecting the potentially important contribution of small ice shelves (discussed in, e.g. Timmermann et al., 2012) and ice shelf teleconnections (Gwyther et al., 2014; Silvano et al., 2018). Also, inconsistent design and parameter choices make it difficult to identify the governing processes on a continent-wide scale. In contrast, Ocean General Circulation Models (OGCMs) that have global coverage and include tidal currents have not been extended to include by an ice shelf component (Savage et al., 2017; Stewart et al., 2018). To our best knowledge, no Antarctic-wide ocean model that resolves ice shelf interactions and tides simultaneously has so-far been developed (Asay-Davis et al., 2017). Here, using an Antarctic-wide ocean-ice shelf model that explicitly resolves tides, we quantify the impact of tidal currents on ice shelf basal melting and the continental shelf seas. Further, we derive insights into the governing mechanisms that drive tidal melting by performing a dynamical-thermodynamical decomposition of the melt drivers at the ice shelf base (similar to Jourdain et al., 2019).

The following section (Sect. 2) describes the model, experiments and analysis techniques used in this study. Section 3 presents the results. First, we show tide-induced annual mean changes in ice shelf melting and the continental shelf seas. Second, we present the outcome of the decomposition analysis. The results section is followed by a discussion of the implications for larger scale modelling efforts that include ice sheets and global oceans (Sect. 4). The last section (Sect. 5) summarises the study and presents its conclusions.

2 Methods

2.1 Model Description

We derive estimates of ice shelf-ocean interaction using the Whole Antarctic Ocean Model (WAOM) at 4 km horizontal resolution (Richter et al., 2020). The reference simulation performed for this study is similar to the experiment described and evaluated by Richter et al. (2020), except for the horizontal resolution (Richter et al., 2020 evaluates the 2 km version of the model). At 4 km horizontal resolution, we resolve the tidal processes critical for the focus of this study (as discussed in

Richter et al. (2020)). In the following we reiterate the key points of WAOM and describe the experiments performed here. The model is based on the Regional Ocean Modeling System (ROMS) version 3.6 (Shchepetkin and McWilliams, 2005), which uses terrain-following vertical coordinates, and has been augmented by an ice shelf component (Galton-Fenzi et al., 2012). Thermodynamic ice-ocean interaction is described using the three equation melt parameterisation (Hellmer and Olbers, 1989; Holland and Jenkins, 1999) including velocity dependent exchange coefficients (McPhee, 1987) and a modification that ensures a weak exchange in the case of zero velocity (due to molecular diffusion; see Gwyther et al., 2016).

The domain covers the entire Antarctic continental shelf, including all ice shelf cavities (as shown in Fig. 1). The bathymetry and ice draft topography has been taken from the Bedmap2 dataset (Fretwell et al., 2013), while boundaries for 139 individual ice shelves are based on the MEaSURES Antarctic boundaries dataset (Mouginot et al., 2016). A well known feature of terrain following coordinates are pressure gradient errors in regions of steep sloping topography, ultimately driving spurious circulation patterns (Mellor et al., 1994, 1998). To minimise pressure gradient errors in WAOM, we smooth the ice draft and bottom topography using the Mellor-Ezer-Oey algorithm (Mellor et al., 1994) until a maximum Haney factor of 0.3 is reached (Haney, 1991). Further, we artificially deepen the seafloor to a minimum water column thickness of 20 m to ensure numerical stability (see Schnaase and Timmermann, 2019, for implications). The ocean is discretised using a uniform horizontal grid spacing of 4 km and 31 vertical levels with enhanced resolution towards the surface and seafloor. Running the model for one year with 2304 CPUs on 2x8 core Intel Xeon E5-2670 (Sandy Bridge) Nodes costs about 7000 CPU-hours.

2.2 Simulations

For this study we perform two model simulations with ocean-atmosphere-sea ice conditions from the year 2007, one with tidal forcing and one without tides. We force the tidal run with 13 major constituents (M2, S2, N2, K2, K1, O1, P1, Q1, MF, MM, M4, MS4, MN4) derived from the global tidal solution TPXO7.2 (Egbert and Erofeeva, 2002) as sea surface height and barotropic currents along the northern boundary of the domain (north of 60 °S). In this way we achieve an accuracy in the tidal height signal around the coast of Antarctica that is comparable to available barotropic tide models (assessed in King and Padman, 2005; see Richter et al., 2020, their Table 2). At 10 km horizontal resolution WAOM has a combined root-mean-square error in the complex expression of tides of 20 cm, compared to the continent-wide Antarctic Tide Gauge record (Padman et al., 2020). Evaluating tides at higher resolution would have taken considerably more resources and we expect the improvement in accuracy with finer grid spacing to be incremental. For more information about the accuracy of WAOM's tides, including the spatial distribution, see Richter et al. (2020).

Open boundary conditions and surface fluxes are identical in both simulations. The ocean outside the model domain is described using the ECCO2 reanalysis (Menemenlis et al., 2008) and includes monthly averages of sea surface height, barotropic and baroclinic velocities, temperature and salinity. At the surface, daily wind stress is calculated by applying a bulk flux formula to ERA-Interim 10-m winds (Dee et al., 2011). We prescribe daily heat and salt fluxes, which have been derived using satellite sea ice data and heat flux calculations (Tamura et al., 2011). Prescribing surface buoyancy fluxes rather than including a sea ice model has the advantage of accurate surface salt flux location and strength from sea ice polynyas, but does not allow for sea ice-ocean interaction (see discussion by Richter et al., 2020). In addition, a small correction term is added to the heat

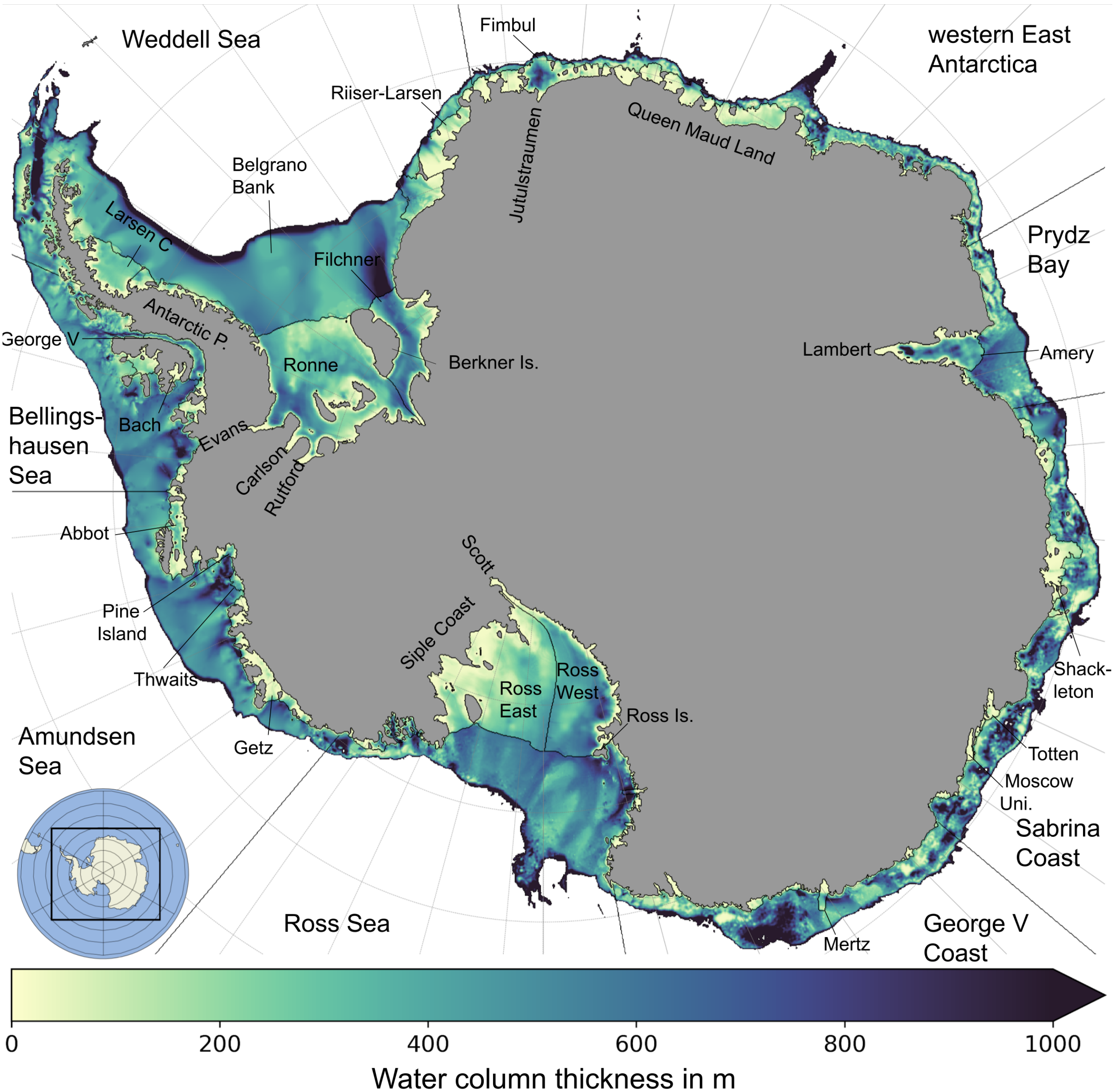

Figure 1. Study area and water column thickness on the continental shelf. Colours show the seafloor depth on the open continental shelf and water column thickness where ice shelves are present. The labels indicate locations referred to in the text with ice sheet regions and tributary glaciers on land, and ice shelves and ocean sectors on water. Abbreviations are Island (Is.), Ice Rise (I.R.) and Peninsula (P.). Inlet shows model boundaries.

and salt fluxes to constrain model drift over annual time scales. These corrections are based on the difference between the model's solution of surface temperature and salinity compared to monthly estimates from the Southern Ocean State Estimate reanalysis (Mazloff et al., 2010). Furthermore, we ensure that positive salt flux from sea ice formation occurs only when sea surface temperatures are at or below freezing. We do not account for the effect of sea ice on wind stress or include an explicit model of frazil ice (as in, e.g. Galton-Fenzi et al., 2012).

Initial temperatures and salinities are also derived from ECCO2, whereby we extrapolate values under the ice shelves from ice front conditions. The tidal and non-tidal case were run separately for 5 years using a 10 km version of the model followed by 2 years at 4 km resolution. By performing parts of the spin up at lower resolution, we save computational costs, while still ensuring a quasi-equilibrium of the continental shelf seas (measured using Antarctic average melting; see Richter et al., 2020, their Fig. 2). Annual average and decomposition results were derived from the final year of the 4 km simulations, while mean tidal current speed was based on an additional subsequent 30-day integration (January) of the tidal case.

2.3 Analysis

We derive an estimate of mean tidal current speed ($|u|_{tide}$). First, we separate the tidal signal from the two orthogonal barotropic velocity components by means of high-pass filtering ($u_{b,HP}$ and $v_{b,HP}$) and, second, we calculate the velocity magnitude from these filtered components as:

$$|u|_{tide} = \left\langle \sqrt{u_{b,HP}^2 + v_{b,HP}^2} \right\rangle_t \qquad [\mathrm{m\ s^{-1}}]\ . \tag{1}$$

The temporal average (subscript t) is taken over 30 days of hourly snapshots. The high-pass filter uses a cut-off frequency of 25 hours, which has been shown to effectively separate most of the high frequency variability associated with tides (Stewart et al., 2018). With 30 days we cover 2 full spring-neap cycles of the major semidiurnal and diurnal tidal constituents M2, S2, K1 and O1. Tidal currents typically reach a maximum speed of 2 $|u|_{tide}$.

We perform a dynamical-thermodynamical decomposition to explore the mechanisms that govern tidal melting in our simulation (similar to Jourdain et al., 2019). The main characteristics of ice shelf basal melting as derived from the three equation melt parameterisation (w_b) can be approximated using the covariance of friction velocity (u^*) and thermal driving (T^*, see Holland and Jenkins, 1999):

$$w_b\ [\mathrm{m\ yr^{-1}}] \quad \propto \quad u^* T^*\ [\mathrm{m\ s^{-1}} {}^\circ C]\ . \tag{2}$$

The friction velocity controls the exchange rates of heat and salt through the boundary layer and is calculated using the surface quadratic stress:

$$u^* = \sqrt{C_d(u_{top}^2 + v_{top}^2)} \qquad [\mathrm{m/s}]\ . \tag{3}$$

Here, C_d is a quadratic drag coefficient and u_{top} and v_{top} are the orthogonal velocities components of the uppermost sigma layer. Thermal driving is defined as the difference in temperature across the ice-ocean boundary layer:

$$T^* = T_M - T_B \quad [^\circ C] \,, \tag{4}$$

where T_M is the temperature in the top model cell (approximately 0.3 m to 5.0 m below the ice base; assumed to be in the 'mixed layer'), while T_B is assumed to be at the insitu freezing point. The approximation of melt rate variability using friction velocity and thermal driving (Eq. 2) allows to decompose melt rate difference between the tidal and non-tidal experiment into a dynamical, thermodynamical and covariational component (equivalent to Jourdain et al., 2019, their Eq. 5):

$$\begin{aligned} w_{b,T} - w_{b,NT} &\propto \overline{u^*_T T^*_T} - \overline{u^*_{NT} T^*_{NT}} \\ &= \overline{(u^*_{NT} + \Delta u^*)(T^*_{NT} + \Delta T^*)} - \overline{u^*_{NT} T^*_{NT}} \\ &= \overline{u^*_{NT} \Delta T^*} + \overline{\Delta u^* T^*_{NT}} + \overline{\Delta u^* \Delta T^*} \,. \end{aligned} \tag{5}$$

Here, the overbar denotes temporal averaging and the Δ describes the difference between the tidal (T) and non-tidal run (NT):

$$\begin{aligned} \Delta u^* &= u^*_T - u^*_{NT} \\ \Delta T^* &= T^*_T - T^*_{NT} \,. \end{aligned} \tag{6}$$

We have applied this decomposition to key regions around Antarctica using one year of hourly averages. The individual terms offer a priori a good physical interpretation. The dynamical component describes the mean effect of tidal current velocity as well as tidal residual flow (including tide induced buoyant plumes from melting upstream). Thermodynamical changes account for tidal vertical mixing of heat below the turbulent boundary layer (TBL) as well as upstream thermal effects associated with tides (including tidal modulation of meltwater input). The local and instantaneous interplay of thermal forcing and friction velocity via melting is captured by the covariational term.

3 Results

3.1 Mean Changes in Ice Shelf Melting and Shelf Seas

The area-integrated impact of tides on modelled annual-average melting and continental shelf seas temperatures is small, as shown in Table 1. The total basal mass loss increases by 4 % when including tides in the model, while ocean temperatures slightly drop (calculated as volume average of the entire ocean south of the 1000 m isobath).

The effects of tides on individual ice shelves, however, can be large. Figure 2 presents the spatial distribution of ice shelf melting around Antarctica as well as the sensitivity of these melt rates to tides. Tides modulate melting all around the continent (Fig. 2c), but impact ice shelf integrated mass loss mostly in cold regions where ambient melt rates are small (e.g. Filchner,

	Without tides	With tides	Difference
Average melt rate	0.90 m/yr	0.93 m/yr	0.04 m/yr
Basal mass loss	1388 Gt/yr	1445 Gt/yr	57 Gt/yr
Continental shelf potential temperature	-1.38 °C	-1.42 °C	-0.04 °C

Table 1. Tide induced difference in area averaged melt rate, basal mass loss and continental shelf seas temperatures for all Antarctic ice shelves (averaging Fig. 2c and Fig. 4). Continental shelf temperatures have been calculated including the sub-ice shelf cavities and using a depth at the shelf break of 1000 m.

Ronne, Ross and Larsen C Ice Shelf; Fig. 2b and 2a). The Ronne Ice Shelf features by far the highest increase in mass loss (44 Gt/yr, 128 %; see Table A1), only in part compensated by reduced melting under the adjacent Filchner Ice Shelf (-8 Gt/yr, -60 %). Modulation at model resolution (4 km) has a standard deviation of 352 % (not shown). Areas of increased melting are often close to areas of reduced melting or increased marine ice accretion, leading to smaller effects when considering ice shelf area averages.

These small scale impacts can often be linked to local tidal current strength. Figure 3 shows the barotropic currents associated with tides. These currents include the annual mean circulation (Fig. 3a) and the mean tidal current strength (Fig. 3b; calculated following Eqn. 1; see Section 2.3). Figure 4a shows the sensitivity of the mean circulation to tides. The sub-ice shelf cavities can be very narrow where streams of grounded ice drain into the large cold water ice shelves, for example, near Evans Ice Stream, Carlson Inlet and Rutford Ice Stream under the Ronne Ice Shelf, near the Lambert Glacier under the Amery Ice Shelf and near Scott Glacier under the Ross Ice Shelf (as shown in Fig. 1). Tidal currents are stronger in these thin water columns near grounding lines (Fig. 3b) and often act to strengthen the ice pump mechanism (Lewis and Perkin, 1986) with enhanced melting at depth followed by reduced melt rates (or increased refreezing) along western outflow regions (Fig. 2c). A similar pattern is also apparent under Fimbul Ice Shelf, where a melt rate increase near the grounding line of the Jutulstraumen Glacier coincides with reduced melt rates all along its keel (Fig. 2c). We note that we artificially deepened the bathymetry in narrow grounding zones and all of the regions mentioned above are affected by this procedure (see Section 2.1). We also note that peaks in tidal velocity away from the grounding zones are often associated with localised melt rate increases, for example, underneath Riiser-Larsen Ice Shelf and the ice shelves of Queen Maud Land, but also in the Amundsen-Bellingshausen Seas underneath the Getz, Abbot and Bach ice shelves.

The largest modulation of ice shelf integrated mass loss (Ronne Ice Shelf) coincides with the most pronounced feature of tidal residual flow in our simulation. When activating tides in the model, a strong gyre forms on the Weddell Sea continental shelf featuring mean velocities of up to tens of centimeter per second (Fig. 3a) and temperature modulations of up to half a degree Celsius (Fig. 4b). This phenomenon has been attributed to tide-topography interaction over Belgrano Bank (Makinson and Nicholls, 1999). The potential contribution of the gyre to the coherent melt increase under the north-western part of Ronne Ice Shelf (Fig. 2c) is discussed later.

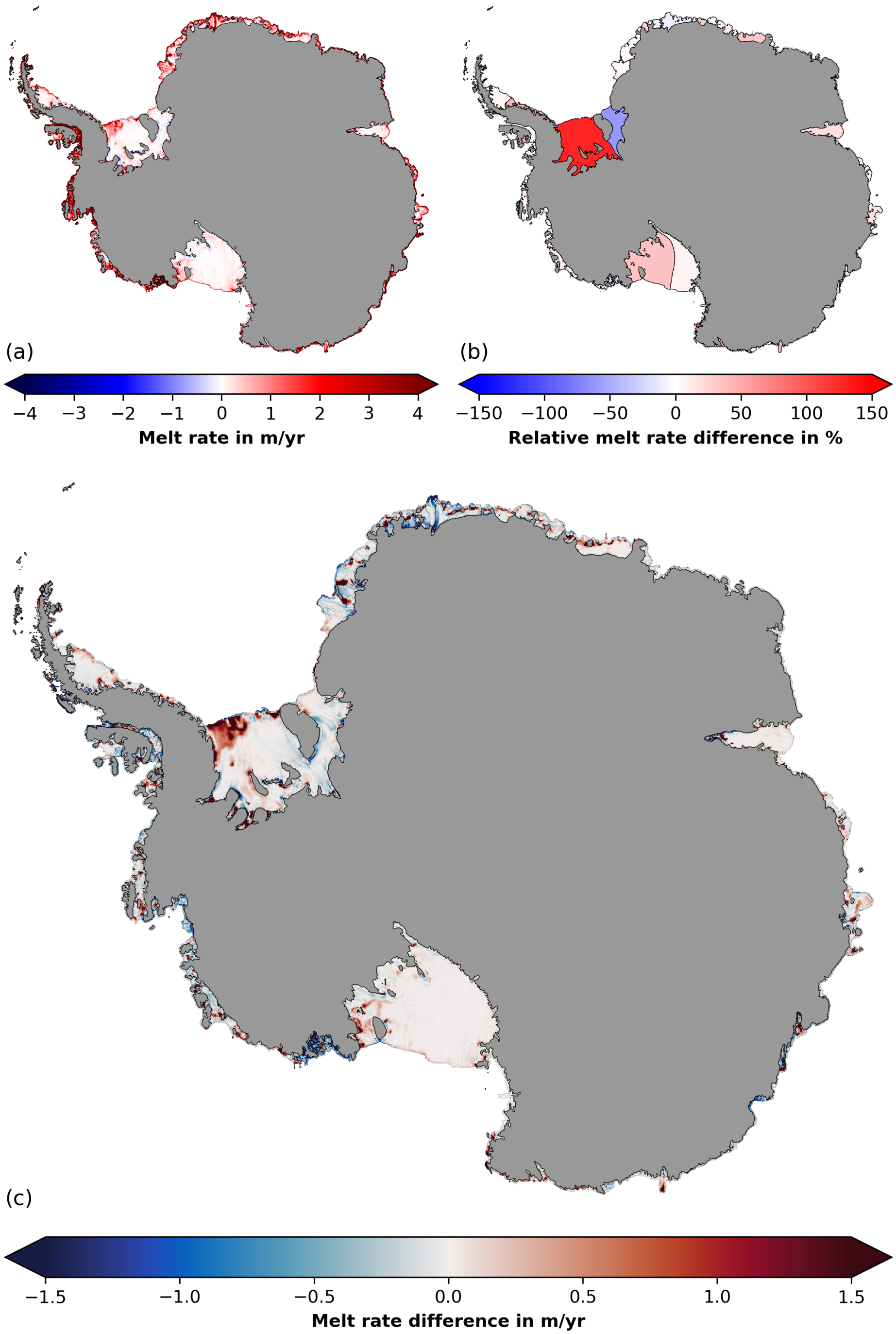

Figure 2. Tidal melting of Antarctic ice shelves. a) Annual average ice shelf melting for the case with tides, b) its relative difference to the case without tides averaged over individual ice shelves ([Tides − No-Tides]/No-Tides) and c) its absolute difference to the case without tides (Tides − No-Tides).

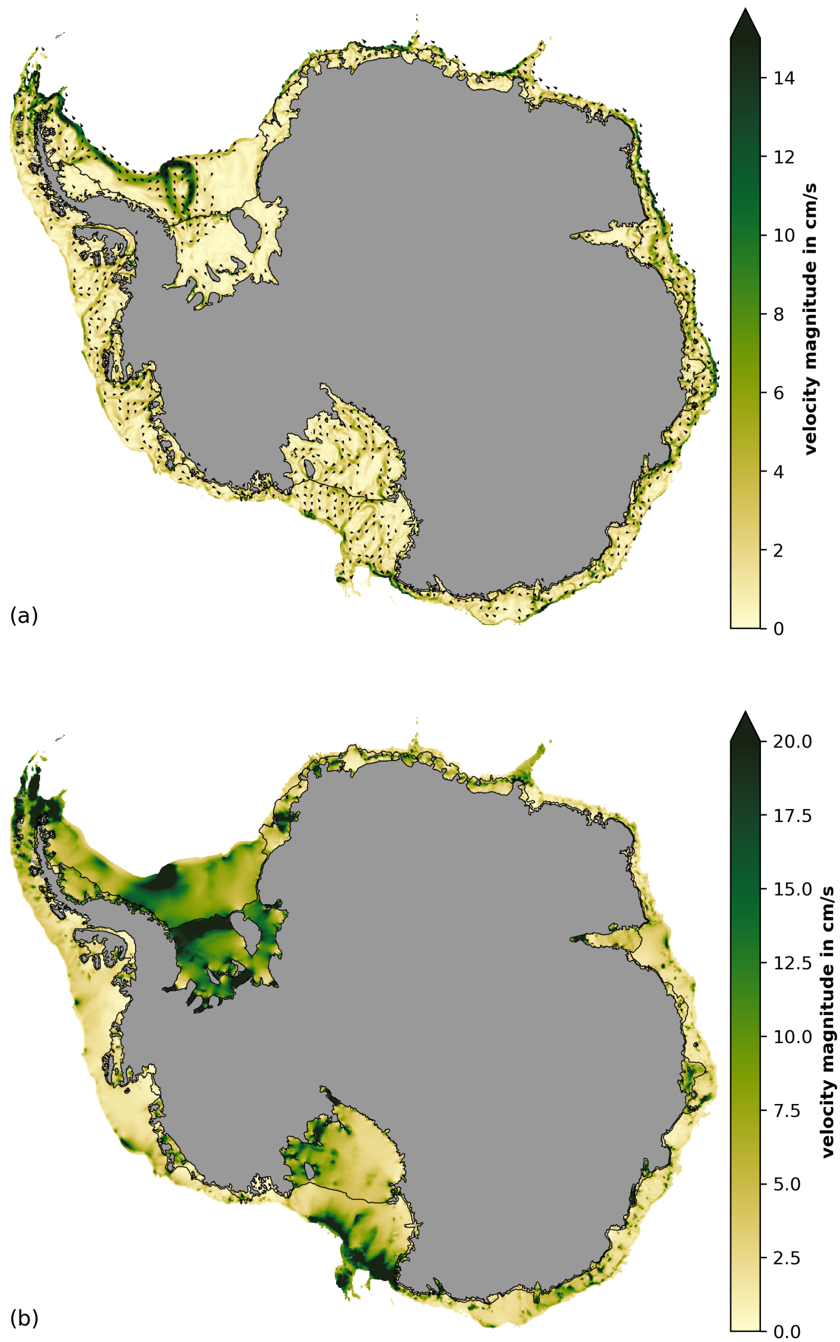

Figure 3. Mean and tidal current speed. a) mean barotropic velocities from the simulation with tides, b) mean speed of oscillating tidal currents ($|u|_{tide}$, calculated following Eqn. 1; see Section 2.3). Arrows in (a) indicate flow direction and are shown only where velocities are stronger than 1 cm/s.

Melting in the frontal parts of ice shelves is often associated with local tidal activity. While our results indicate strong melting at the ice shelf front all around the continent (see Fig. 2a; discussed by Richter et al., 2020), in most regions this melting is independent of tides (as shown in Fig. 2b). Only at few places do tides contribute substantially to melting near ice fronts, for example, west of Berkner Island, east of Ross Island and under the Mertz Glacier tongue. Figure 4 shows the sensitivity of depth averaged continental shelf seas temperature to tides and, in the regions mentioned, adjacent shelf temperatures do not show significant warming. Hence, we attribute near-ice front melting at these locations to tidal advection of solar heated surface waters (proposed by Jacobs et al., 1992; see, e.g. Stewart et al., 2019, for observational evidence).

3.2 Dynamical-Thermodynamical decomposition of tidal melting

We have decomposed the mean impact of tides on ice shelf basal melting into dynamical, thermodynamical and covariational parts (see Sec. 2.3). Figure 5 and 6, respectively, show the results of this decomposition for the Filchner-Ronne Ice Shelf System and the Amundsen Sea ice shelves. The results for other key regions are presented in the supplemental material as Figure B1 to B7.

In most regions, dynamical effects have a major positive contribution to melting or refreezing. These regions also feature elevated tidal current speed (Fig. 3b), and, hence, we associated these changes with tidal currents rather than tidal residual flow (Fig. 4a). Tidal current induced friction, for example, increases melting at shallow grounding zones of cold water ice shelves, in agreement with earlier arguments around the ice pump amplification (e.g. under Filchner-Ronne Ice Shelf , Fig. 5b, along the Siple Coast under Ross Ice Shelf, Fig. B1b, under Larsen C Ice Shelf, Fig. B2b, and under the Amery Ice Shelf, Fig. B3b). In warm regimes dynamic effects are more pronounced at the trunk of ice shelves (e.g. under Bach and Abbot Ice Shelf, Fig. B6b, or under Getz Ice Shelf, Fig. 6b). Generally, where tidal currents are weak, dynamical tidal melting is also less strong (e.g. under the western half of Ross Ice Shelf, in trunk regions of Filchner-Ronne, Amery and Larsen C Ice Shelf, under George V Ice Shelf).

The covariational contribution often opposes dynamical effects (see, e.g. the reversed dipol pattern under Totten Ice Shelf, Fig. B7). This contrasting behaviour can be well explained by friction modulated glacial melt water input at short timescales (hourly in our case; also discussed by Jourdain et al., 2019). In melting regions, dynamically enhanced TBL transport causes heat loss in the uppermost ocean layer and, consequently, reduces thermal driving. In regions of marine ice accretion, the effect is reversed.

In some regions, however, melt rate contributions do not follow this pattern. Under large parts of North-West Ronne Ice Shelf the covariational and dynamical terms are both positive and the covariational contribution is, in part, stronger than the dynamical one. To generate this signature, thermodynamic changes must be taken into account. Indeed, thermodynamic changes are slightly positive despite increased meltwater input from dynamical effects. This thermodynamical contribution is amplified by tidal current friction, which is strong under the entire frontal zone of Ronne Ice Shelf (Fig. 3), resulting in a strongly positive covariational term.

Thermodynamical changes by itself, however, play a secondary role in cold regimes (e.g. under Filchner-Ronne, Fig. 5c, or Ross Ice Shelf, Fig. B1c). In warm regions, thermal effects can be more relevant and mostly reduce melt (see, e.g., Pine

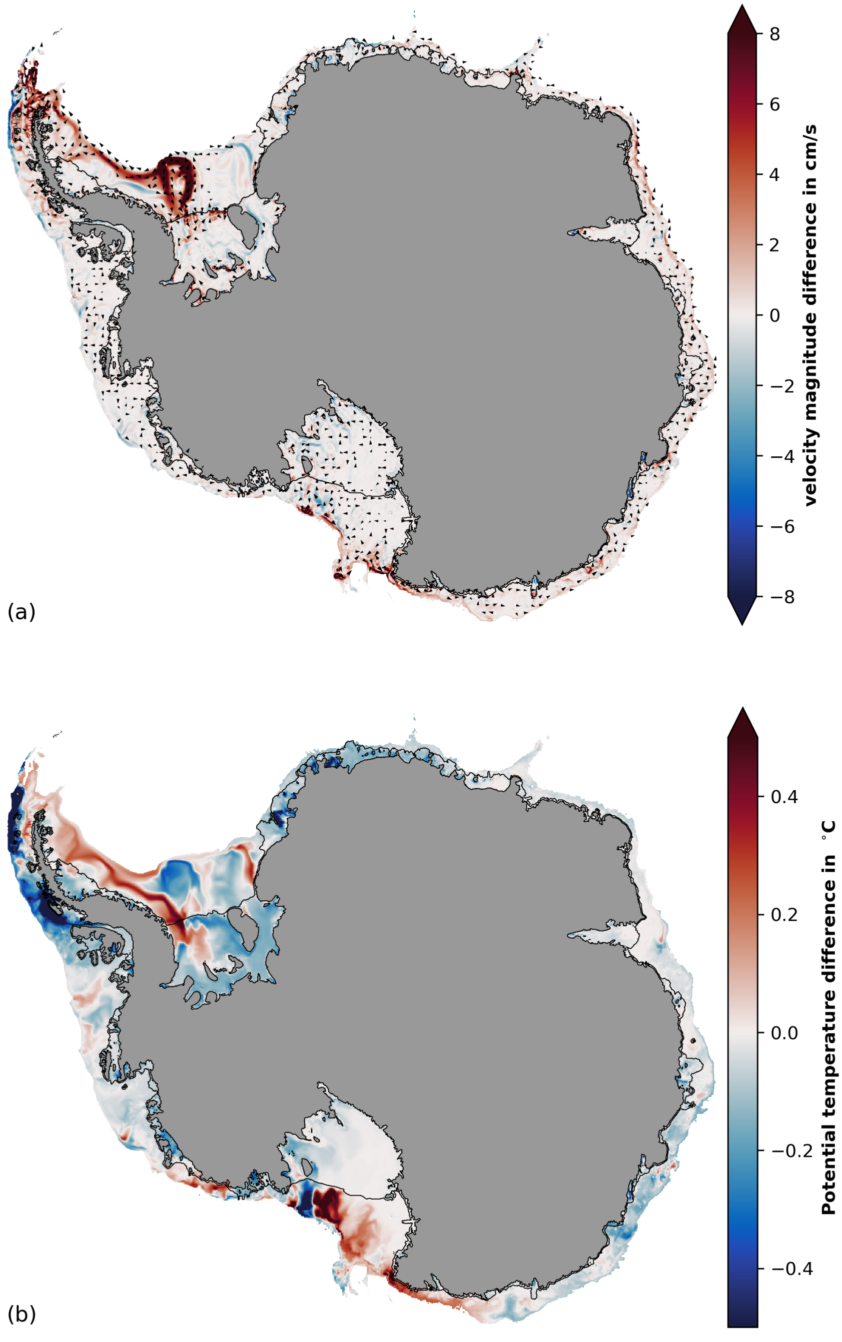

Figure 4. Tide induced change in (a) continental shelf barotropic velocity and (b) potential temperature. Differences show impact when activating tides in the model (Tides – No-Tides)). Arrows in (a) are shown only where velocity change is larger than 1 cm/s.

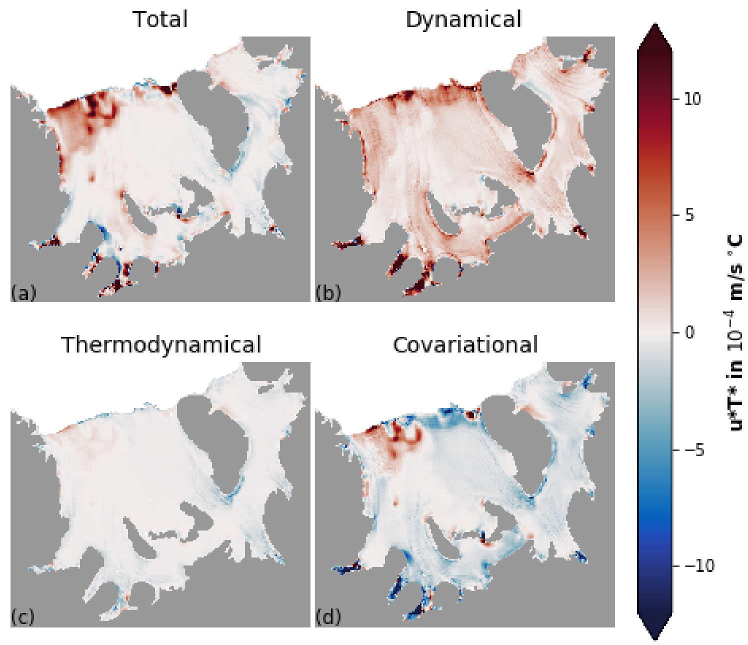

Figure 5. Dynamical-Thermodynamical decomposition of tidal melting under Filchner-Ronne Ice Shelf. Difference in melting, when accounting for (a) all components, (b) only the dynamical component, (c) only the thermodynamical component and (d) only the covariational component (following Eq. 5).

Island, Thwaites and eastern Getz Ice Shelf in the Amundsen Sea, Fig. 6c and all ice shelves in the Bellingshausen Sea, Fig. B6c). This is also the case for the deep glacier keels within the Fimbul (Fig. B4c) and Shackleton Ice Shelf (Fig. B5), which are in contact with relatively warm water in our simulation (Fig. 2a). This cooling might be in part a consequence of increased meltwater input from tidal current enhanced TBL transport (similar to the covariational effect; see, e.g. eastern Getz Ice Shelf, Fig. 6, and Moscow University Ice Shelf, Fig. B7). However, in all of the aforementioned regions the adjacent water on the continental shelf cools with tides (Fig. 4b), supporting that changes in shore-ward heat transport play an important role.

4 Discussion

While circum-Antarctic total melt is small, regional changes in ice shelf melting and continental shelf temperature can be large (up to orders of magnitude and half a degree Celsius, respectively) with potential implications for ice sheet dynamics and AABW formation. The buttressing importance of floating ice can vary by several orders of magnitude within one ice shelf, with regions close to grounding lines, lateral boundaries or pinning points generally being the most important for ice sheet stability (Gudmundsson, 2013; Reese et al., 2018). Our model predicts that the strongest changes in basal mass loss often occur in exactly these parts of the ice shelves. Within these regions, however, increased melting is often in close vicinity to equally

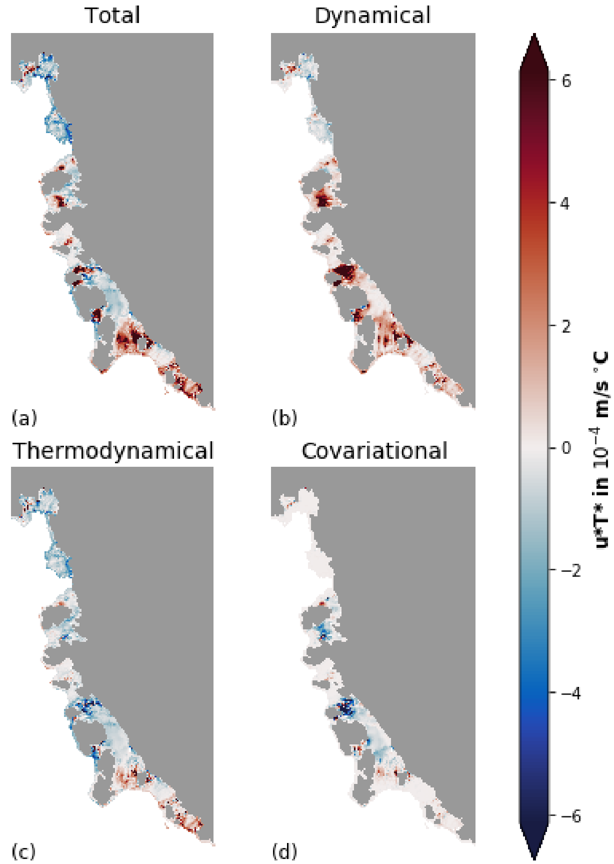

Figure 6. Same as Fig. 5, but for the ice shelves of the Amundsen Sea.

strong reduction in melting or enhanced refreezing, making it difficult to assess the overall impact on buttressing. Diagnostic experiments with ice sheet flow models could be used to quantify the instantaneous response of tide-driven ice shelf thinning on the ice flux across the grounding lines (similar to experiments by Reese et al., 2018). Such approaches, however, do not include longer term consequences.

Antarctic tides are sensitive to changes in ice shelf geometry and sea levels, offering potential feedback on ice sheet relevant timescales. Antarctic tides can be interpreted as waves that propagate around the continent and barotropic ocean models show that shifts in sea levels, grounding line location and ice draft depth significantly alters their propagation and dissipation (Griffiths and Peltier, 2009; Rosier et al., 2014; Wilmes and Green, 2014). Ice shelf retreat in simulations by Rosier et al. (2014), for example, produces an overall increase in M2 dissipation by more than 40 % (see their Table 1). In our simulation, tides act to slightly increase the overall efficiency of the use of ocean heat for ice shelf melting, a finding supported by idealized simulations by Gwyther et al. (2016). How this conversion efficiency responds with stronger tides is unknown. On a more regional scale, tidal current strength is very sensitive to local changes in the water column thickness, which is set by ice shelf geometry and ocean depth (e.g. Galton-Fenzi et al., 2008; Mueller et al., 2012). Mueller et al. (2018) revealed that slight changes in the draft of the Filchner-Ronne Ice Shelf impacts tide driven melting in areas relevant for inland ice sheet dynamics. Therefore, potential positive and negative feedback between ice geometry, basal melting, and local as well as far field tides will need to be explored using coupled ocean-ice shelf-ice sheet models with Antarctic-wide coverage.

Likewise, regional changes in coastal hydrography due to tides might impact water mass transformation with consequences for global oceans and climate. Brine rejection in sea ice polynyas drives the formation of dense water, which has been linked to Antarctic Bottom Water (Purkey and Johnson, 2013) and the meridional overturning circulation (Jacobs, 2004, e.g.). Deep water formation seems to be sensitive to local changes in the ocean, as recent studies show that glacial melt water can offset the densification by polynya activity (Williams et al., 2016; Silvano et al., 2018). Activating tides in our model changes depth average temperatures by up to half a degree Celsius in some locations and generates rectified currents with velocities of up to tens of centimetres per second. The relevance of tide driven currents and temperature changes for water mass formation and transformation on the Antarctic continental shelf, and indeed on the global oceans and climate, is yet to be explored.

Tides are understood to be critically important for ocean-ice shelf interaction (e.g. Galton-Fenzi et al., 2012; Padman et al., 2018), but explicitly resolving tides in larger scale models is expensive. Hence, several studies have developed or applied parameterisations of tidal melting (see, e.g. Jenkins et al., 2010; Hattermann et al., 2014; Asay-Davis et al., 2016; Jourdain et al., 2019). Jourdain et al. (2019) accounts for tide-driven changes in modelled melting of the Amundsen Sea ice shelves by adding a tidal component to the description of the friction velocity (following Jenkins et al., 2010; similar to enhancing bottom drag in non-tide-resolving estuary models). Using this approach, they reproduce not only the dynamical, but also the thermodynamical and covariational effects of tides on melting, showing that the latter two are a consequence of changes in meltwater input from modulated friction in their simulation. In our study, the dynamical component also plays an important role in most regions and covariational effects can, to a large degree, be explained as a dynamical consequence (see Fig. 5 and 6).

In some regions, however, thermodynamic drivers govern the melt change. In particular, we have attributed the coherent melt increase under North-West Ronne Ice Shelf to temperature modulations outside the TBL. These changes might originate from an ocean warming that spans across the ice shelf front, associated with a tide-topography gyre on the adjacent continental shelf (Fig. 4). However, tidal vertical mixing (below the TBL) is also known to be strong here (see Makinson and Nicholls, 1999; in agreement with our tidal current strength, Fig. 3). The strength of the gyre is very uncertain (Makinson and Nicholls, 1999) and a warm bias in WAOM might overestimate its importance for melting. We suggest further investigations are required into the role of the gyre for Filchner-Ronne Ice Shelf melting using a regional model, e.g. based on the ROMS configuration developed by Mueller et al. (2018) with northern boundaries extended up to the continental shelf break. Any melt rate modulation that is indeed induced by the gyre or tidal mixing will not be captured by accounting for dynamical tidal effects on the TBL alone. Overall, the results from this study motivate a direct assessment of the tidal melt parameterisation described by Jourdain et al. (2019) in a pan-Antarctic context. WAOM would be well suited to perform these experiments.

The major limitation of this study has its roots in the early development stage of the underlying ocean model. WAOM v1.0 qualitatively reproduces the large-scale characteristics of Antarctic ice shelf-ocean interaction, but biases have also been identified (Richter et al., 2020 open access review), limiting the quantitative conclusions that can be drawn regarding the tidal sensitivity. A warm bias on the western Weddell Sea continental shelf, for example, might lead to an overestimation of the here reported tide driven melting under North-West Ronne Ice Shelf (see Richter et al., 2020 their Figure 9). Likewise, a cold bias on the Amundsen-Bellingshausen Seas continental shelf potentially leads to an overestimation of tidal melting driven by thermodynamic effects in this region. Further, sea ice interacts with ice shelf melting (e.g. Hellmer, 2004; Silvano et al., 2018) and tides (Padman et al., 2018), and our approach does not account for these interactions, potentially missing important feedbacks. In the light of these limitations, this study should be seen as a first large scale investigation into a process potentially important for sea level rise and global climate. We encourage research groups using other pan-Antarctic ocean-ice shelf applications to implement tides and repeat the experiments of this study.

Future studies that aim to apply WAOM, for example to past or future periods, should calibrate vertical tidal mixing first. The tide-induced changes in continental shelf temperature (Fig. 4b) show some similarity with the reported biases (Richter et al., 2020 their Fig. 9), hinting towards a connection. Richter et al. (2020) has also identified overly mixed conditions on the continental shelf and linked these to the temperature biases (via erosion of warm deep water in the Amundsen Sea and missing HSSW formation in the Weddell Sea). Tidal mixing is sensitive to the choice of the vertical mixing parameterisation in ROMS and, while the configuration used by WAOM v1.0 has been established in several regional studies (Galton-Fenzi et al., 2012; Cougnon et al., 2013; Gwyther et al., 2014), there is evidence that the applied mixing scheme (KPP) overestimates tidal vertical mixing (Robertson and Dong, 2019; Robertson, 2006).

5 Summary and Conclusion

This study provides a first estimate of tide driven ice shelf basal melting in an Antarctic-wide context. Activating tides in the model increases total mass loss by 4 % and mass loss modulations for most ice shelves are below 10 %. The Ronne-Filchner Ice Shelf system exhibits larger coherent changes (Ronne melt increases by 128 %), potentially related to a strong tide induced gyre over Belgrano Bank. Melt rate modulation at smaller scales can exceed 100 % in cold regimes and are in part located near grounding lines and lateral boundaries, regions important for ice shelf buttressing. The ocean temperature of the entire continental shelf decreases by only 0.04 °C. Regional modulations can exceed 0.5 °C including a strong warming of the Western Weddell Sea.

Dynamical-thermodynamical decomposition of tidal melting highlights the importance of tidal current enhanced exchange rates of heat and salt in the TBL. This motivates future studies to assess available tidal melt parameterisations (e.g. by Jourdain et al., 2019) to the pan-Antarctic domain. Thermodynamic driven changes due to mixing or residual flow play a role in some regions, but might be overestimated due to biases in the control run.

The strong regional sensitivity of ice shelf melting and continental shelf temperatures in our simulation highlights the need to investigate the impact of tides on ice sheet dynamics and AABW formation over glacial time scales.

Code and data availability. The source code and configuration files used for the simulations described here are archived at http://doi.org/10.5281/zenodo.3738985 (Richter, 2020a), while the maintained version is publicly available at https://github.com/kuechenrole/waom. The raw model output, grid files, atmospheric forcing, initial conditions, and northern boundary conditions can be obtained from the authors upon request. The data underlying the figures of this study are available at http://rdp.utas.edu.au/metadata/d34f18f9-a878-49cb-9ad5-b4d27e0c7b77. The Python and Matlab scripts used to generate the grid and forcing files and to perform the analysis on the model output are archived at http://doi.org/10.5281/zenodo.3738998 (Richter, 2020b) and the maintained version of these scripts is publicly available at https://github.com/kuechenrole/antarctic_melting.

Appendix A: Tide-Driven Ice Shelf Basal Mass Loss

Table A1. Ice shelf average mass loss due to tides. For 139 individual ice shelves the table shows the area, melt rate (w_b) and Basal Mass Loss (BML) of the run with tides as well as its difference to the run without tides in absolute (e.g. $w_{b\text{ tides}} - w_{b\text{ no-tides}}$) and relative ($(w_{b\text{ tides}} - w_{b\text{ no-tides}})/w_{b\text{ no-tides}}$) terms. Ice Shelf boundaries have been taken from the MEaSURES dataset (Mouginot et al., 2016).

Ice Shelf	**Area** (10^3km^2)	w_b **(m/yr)**	**BML (Gt/yr)**	w_b **Difference (m/yr)**	**BML Difference (Gt/yr)**	w_b **and BML Relative Difference (%)**
Abbot	29.74	2.57	70.09	0.14	3.95	5.97
Abbot 1	0.24	1.11	0.24	-0.05	-0.01	-4.50
Abbot 2	0.34	0.92	0.28	-0.02	-0.01	-2.23
Abbot 3	0.35	0.39	0.13	-0.01	0.00	-2.31
Abbot 4	0.43	1.34	0.53	-0.02	-0.01	-1.53
Abbot 5	0.54	1.23	0.61	0.03	0.02	2.77
Abbot 6	0.26	0.65	0.15	-0.01	0.00	-1.91
Ainsworth	0.12	0.40	0.05	0.00	0.00	-0.20
Alison	0.08	6.66	0.49	-0.37	-0.03	-5.25
Amery	59.85	0.18	9.68	0.03	1.59	19.73
Astrolabe	0.11	0.72	0.07	-0.07	-0.01	-8.80
Atka	2.14	1.34	2.62	0.12	0.23	9.50
Aviator	0.92	0.26	0.22	0.03	0.02	11.48
Bach	4.61	3.49	14.74	1.11	4.70	46.80
Baudouin	33.40	0.74	22.62	0.18	5.55	32.53
Borchgrevink	21.11	1.51	29.15	0.12	2.27	8.46
Brahms	0.25	2.00	0.47	-0.04	-0.01	-2.15
Brunt Stancomb	36.66	1.03	34.63	0.05	1.65	4.99
Campbell	0.11	0.73	0.08	0.00	0.00	0.09
Cheetham	0.11	0.11	0.01	0.00	0.00	0.76
Chugunov	0.05	0.66	0.03	0.12	0.01	22.72
Conger Glenzer	1.63	3.08	4.58	0.72	1.08	30.78
Cook	3.63	3.72	12.38	-0.18	-0.61	-4.71
Cosgrove	2.94	3.40	9.16	0.13	0.35	4.00
Crosson	3.11	0.69	1.98	-0.05	-0.14	-6.59
Deakin	0.09	2.60	0.22	-0.28	-0.02	-9.64
Dennistoun	0.13	1.40	0.16	0.82	0.10	143.73
Dibble	1.56	2.81	4.01	0.12	0.18	4.59

continued on next page

continued from previous page

Ice Shelf	**Area** (10^3km^2)	w_b **(m/yr)**	**BML (Gt/yr)**	w_b **Difference (m/yr)**	**BML Difference (Gt/yr)**	w_b **and BML Relative Difference (%)**
Dotson	5.16	0.70	3.33	-0.04	-0.18	-5.21
Drury	0.09	1.56	0.13	0.35	0.03	29.10
Drygalski	2.45	0.73	1.63	0.06	0.13	8.72
Edward VIII	0.43	0.56	0.22	-0.03	-0.01	-4.32
Ekstrom	6.90	1.06	6.69	0.23	1.45	27.69
Erebus	0.05	0.25	0.01	0.03	0.00	14.75
Ferrigno	0.18	6.43	1.04	-0.49	-0.08	-7.02
Filchner	102.07	0.06	5.51	-0.09	-8.31	-60.14
Fimbul	40.69	1.73	64.31	-0.19	-6.96	-9.77
Fisher	0.19	0.83	0.14	0.03	0.00	3.13
Fitzgerald	0.37	0.29	0.10	0.05	0.02	22.97
Flatnes	0.09	0.53	0.05	0.03	0.00	6.22
Fox Glacier	0.08	3.33	0.23	-0.06	0.00	-1.85
Francais	0.09	1.56	0.13	-0.15	-0.01	-8.80
Frost	0.26	2.33	0.56	-0.95	-0.23	-28.88
Garfield	0.06	0.46	0.03	0.02	0.00	4.00
Geikie Inlet	0.33	0.09	0.03	-0.01	0.00	-7.72
George VI	23.15	7.76	164.50	-0.20	-4.28	-2.53
Getz	33.50	1.95	59.97	0.17	5.33	9.76
Getz 1	0.60	1.09	0.59	-0.17	-0.09	-13.22
Gillet	0.17	0.90	0.14	0.33	0.05	56.87
Hamilton	0.21	2.88	0.56	-0.46	-0.09	-13.65
Hannan	0.40	0.30	0.11	-0.01	0.00	-2.17
Harbord Glacier	0.10	0.14	0.01	0.01	0.00	10.54
Helen	0.35	1.98	0.64	-0.05	-0.02	-2.60
Holmes	2.38	1.56	3.40	-0.73	-1.59	-31.87
Holt	0.08	1.11	0.08	0.28	0.02	33.78
Horn Bluff	0.17	1.67	0.26	0.07	0.01	4.17
Hoseason	0.14	1.15	0.15	0.03	0.00	2.32
Hull	0.19	0.97	0.17	0.02	0.00	2.21
Ironside	0.10	0.20	0.02	0.04	0.00	21.93
Jackson	0.08	0.95	0.07	0.12	0.01	14.47

continued on next page

continued from previous page

Ice Shelf	Area (10^3km^2)	w_b (m/yr)	BML (Gt/yr)	w_b Difference (m/yr)	BML Difference (Gt/yr)	w_b and BML Relative Difference (%)
Jelbart	10.83	1.10	10.96	-0.09	-0.90	-7.58
Land	0.68	3.07	1.92	1.62	1.02	112.06
LarsenA	0.79	0.60	0.44	0.38	0.27	164.36
LarsenB	2.13	0.43	0.83	0.03	0.05	6.82
LarsenC	46.50	0.24	10.17	0.01	0.50	5.20
LarsenD	21.84	0.30	5.96	0.09	1.83	44.41
LarsenD 1	0.06	0.23	0.01	-0.13	-0.01	-35.59
LarsenE	1.25	0.68	0.78	0.29	0.33	74.79
LarsenF	0.87	0.34	0.27	0.12	0.09	51.86
LarsenG	0.47	0.17	0.07	-0.05	-0.02	-21.45
Lauritzen	0.60	2.02	1.10	0.40	0.22	24.98
Lazarev	8.73	0.73	5.80	-0.01	-0.10	-1.74
Lillie	0.86	2.58	2.02	0.26	0.21	11.37
Mariner	2.73	0.69	1.73	0.36	0.90	108.98
Marret	0.05	2.70	0.11	-0.37	-0.02	-12.21
Matusevitch	0.30	4.61	1.26	1.03	0.28	28.72
May Glacier	0.32	2.53	0.75	0.16	0.05	6.77
Mendelssohn	0.48	3.76	1.64	-0.22	-0.09	-5.41
Mertz	5.68	1.40	7.27	0.41	2.13	41.37
Moscow Uni.	6.10	1.38	7.72	-0.24	-1.31	-14.54
Moubray	0.18	0.27	0.04	0.15	0.02	132.46
Mulebreen	0.34	0.52	0.16	-0.03	-0.01	-4.82
Nansen	1.98	0.01	0.02	-0.01	-0.02	-48.74
Nickerson	6.83	3.67	22.93	-0.57	-3.55	-13.42
Ninnis	2.03	2.82	5.25	-0.04	-0.07	-1.23
Nivl	7.53	0.40	2.79	0.09	0.62	28.80
Noll	0.16	4.00	0.58	1.03	0.15	34.55
Nordenskjold	0.29	0.30	0.08	0.02	0.00	6.55
Parker	0.11	0.11	0.01	0.00	0.00	4.78
Philbin Inlet	0.11	0.47	0.05	-0.04	0.00	-8.37
Pine Island	5.96	7.02	38.32	-0.33	-1.78	-4.44
Porter	0.08	2.04	0.14	-0.04	0.00	-1.71

continued on next page

continued from previous page

Ice Shelf	**Area** (10^3km^2)	w_b **(m/yr)**	**BML (Gt/yr)**	w_b **Difference (m/yr)**	**BML Difference (Gt/yr)**	w_b **and BML Relative Difference (%)**
Pourquoi Pas	0.20	4.91	0.90	-0.44	-0.08	-8.25
Prince Harald	5.66	1.27	6.61	-0.04	-0.23	-3.34
Publications	1.62	0.62	0.93	0.07	0.10	12.24
Quar	2.29	1.71	3.59	-0.08	-0.18	-4.66
Rayner Thyer	0.62	0.28	0.16	0.03	0.02	13.32
Rennick	3.32	0.25	0.77	0.08	0.25	48.91
Richter	0.15	7.91	1.07	-0.80	-0.11	-9.19
Riiser-Larsen	43.53	0.93	37.11	0.04	1.63	4.61
Ronne	333.48	0.26	78.32	0.14	43.93	127.75
Ross East	191.24	0.17	29.30	0.01	2.04	7.47
Ross West	300.76	0.16	43.57	0.04	11.41	35.46
Rund Bay	0.14	1.33	0.17	-0.08	-0.01	-5.60
Shackleton	26.43	0.80	19.37	0.10	2.50	14.84
Shirase	0.74	1.33	0.91	-0.01	-0.01	-1.10
Skallen	0.06	0.30	0.02	0.01	0.00	2.65
Slava	0.38	0.75	0.26	0.03	0.01	3.61
Sorsdal	0.19	1.24	0.21	0.03	0.01	2.79
Stange	8.29	2.50	18.98	0.24	1.83	10.66
Sulzberger	12.47	7.81	89.24	-0.96	-10.97	-10.94
Suter	0.05	0.11	0.00	0.07	0.00	172.75
Suvorov	0.22	1.02	0.21	0.18	0.04	20.85
Swinburne	0.93	12.74	10.88	-0.92	-0.78	-6.71
Thwaites	4.51	7.36	30.36	-0.54	-2.22	-6.82
Tinker	0.15	0.03	0.00	-0.01	0.00	-13.99
Totten	6.14	1.72	9.66	0.27	1.50	18.39
Tracy Tremenchus	2.81	0.86	2.20	0.02	0.05	2.46
Tucker	0.46	0.75	0.32	0.42	0.18	125.72
Underwood	0.20	2.26	0.42	-0.09	-0.02	-3.75
Utsikkar	0.09	0.73	0.06	0.01	0.00	1.51
Venable	3.31	4.65	14.07	-0.20	-0.62	-4.20
Verdi	0.14	5.41	0.71	-0.13	-0.02	-2.29
Vigrid	2.10	1.07	2.07	0.03	0.06	3.16

continued on next page

continued from previous page

Ice Shelf	**Area** (10^3km^2)	w_b **(m/yr)**	**BML (Gt/yr)**	w_b **Difference (m/yr)**	**BML Difference (Gt/yr)**	w_b **and BML Relative Difference (%)**
Vincennes Bay	1.14	1.99	2.08	-0.06	-0.06	-2.80
Voyeykov	0.69	1.66	1.06	-0.07	-0.05	-4.29
Walgreen Coast 1	0.11	5.95	0.62	-0.55	-0.06	-8.50
Walgreen Coast 2	0.03	2.84	0.08	-0.40	-0.01	-12.40
Watt Bay	0.11	0.68	0.07	-0.11	-0.01	-13.83
West	15.86	1.69	24.58	0.09	1.35	5.79
Whittle	0.11	1.06	0.10	-0.28	-0.03	-20.75
Wilkins	13.04	1.31	15.61	-0.06	-0.76	-4.65
Williamson	0.20	2.67	0.49	-0.24	-0.04	-8.14
Wilma-Robert-Downer	0.91	0.50	0.42	-0.03	-0.03	-5.72
Withrow	0.72	4.09	2.70	-0.83	-0.55	-16.94
Wordie (Harriott)	0.09	0.12	0.01	-0.02	0.00	-12.46
Wordie (Prospect)	0.20	0.19	0.03	0.00	0.00	-1.19
Wylde	0.18	0.22	0.04	0.08	0.01	58.21
Zubchatyy	0.33	0.80	0.24	-0.07	-0.02	-7.50

Appendix B: Dynamical-thermodynamical decomposition

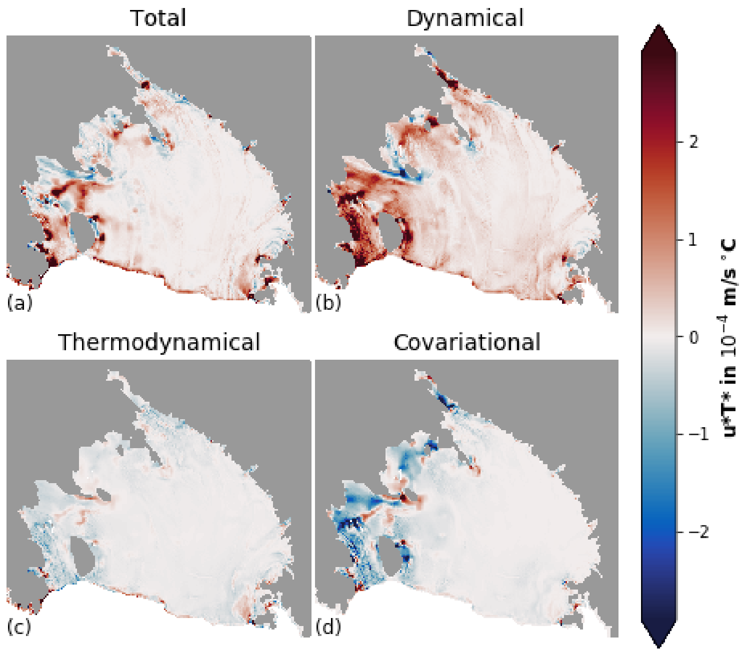

Figure B1. Dynamical-Thermodynamical decomposition of tidal melting under Ross Ice Shelf (same as Fig. 5). Difference in melting, when accounting for (a) all components, (b) only the dynamical component, (c) only the thermodynamical components and (d) only the covariational component (following Eq. 5).

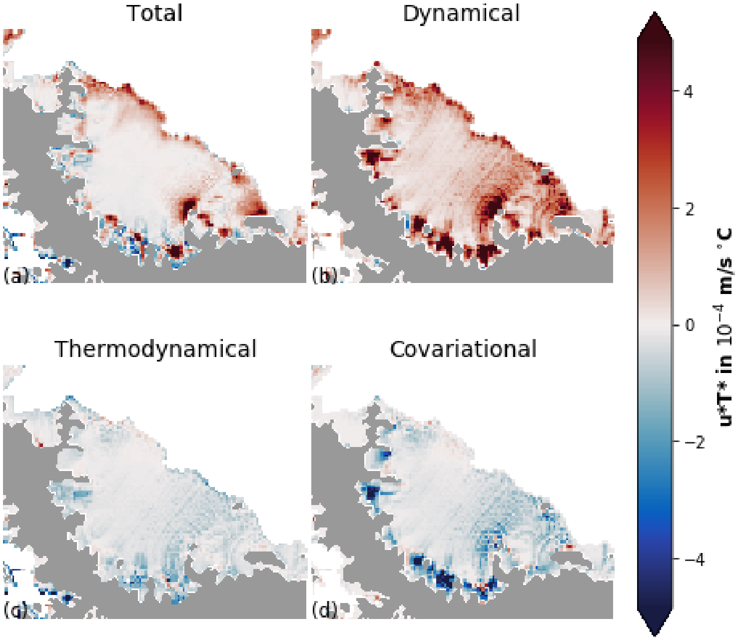

Figure B2. Same as Fig. B1, but for the Larsen C Ice Shelf.

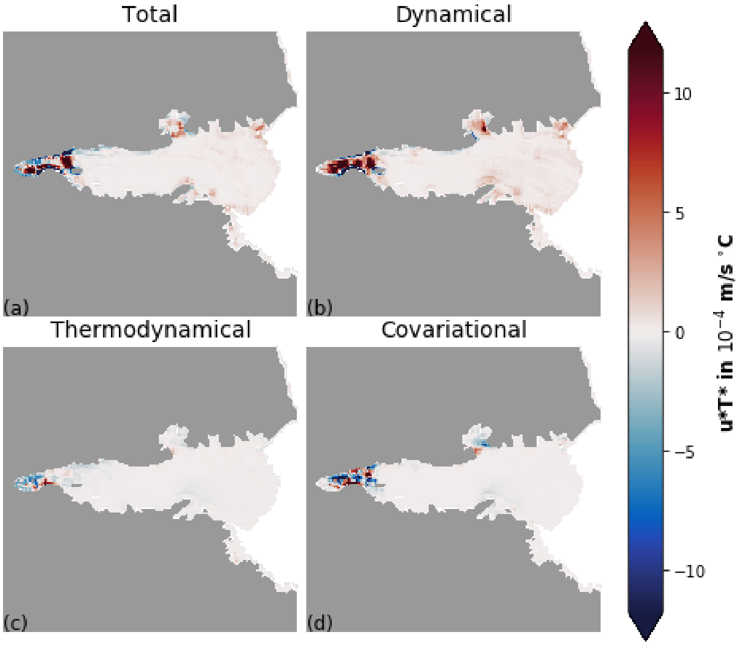

Figure B3. Same as Fig. B1, but for the Amery Ice Shelf.

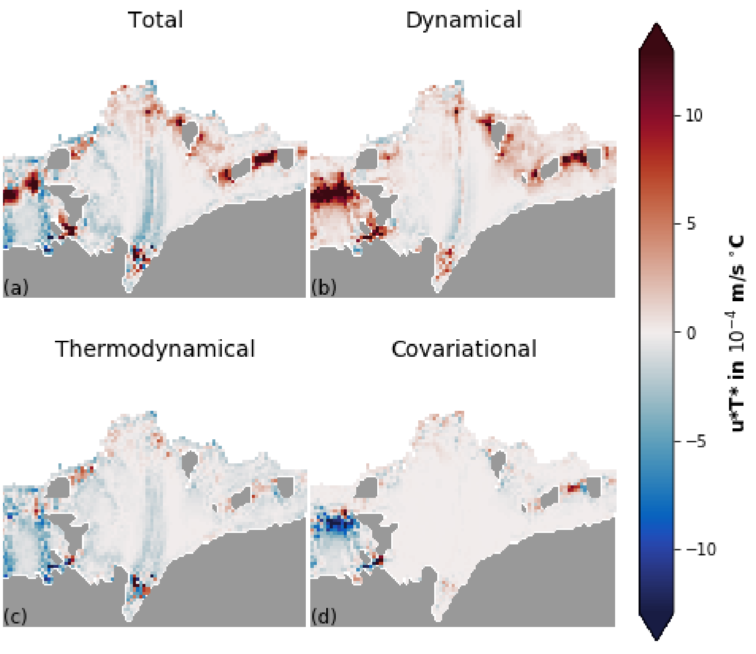

Figure B4. Same as Fig. B1, but for the Fimbul Ice Shelf.

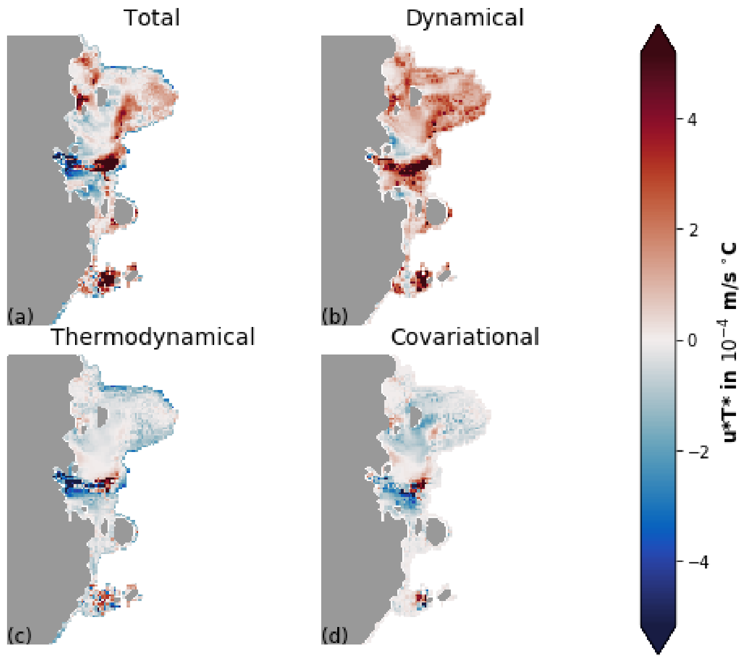

Figure B5. Same as Fig. B1, but for the Shackleton Ice Shelf.

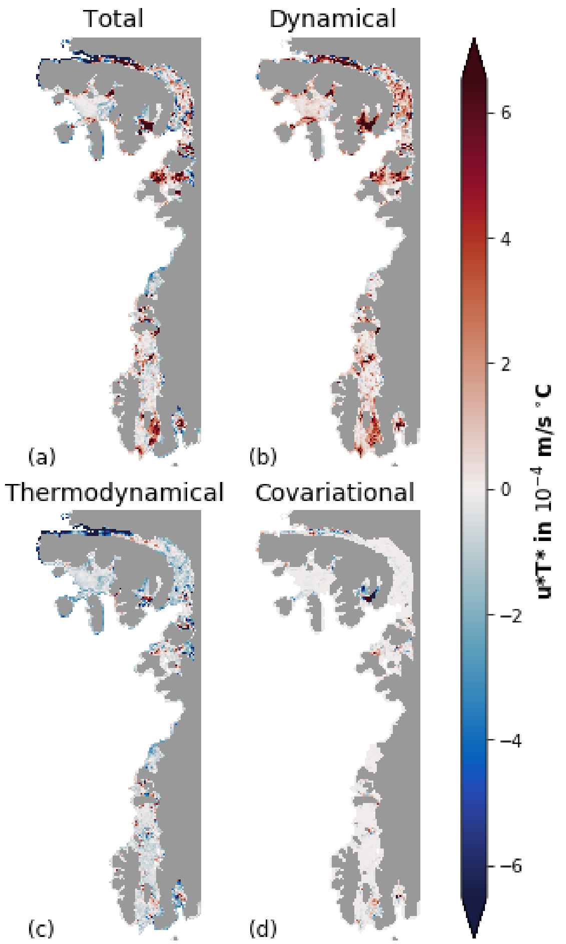

Figure B6. Same as Fig. B1, but for the ice shelves of the Bellingshausen Sea.

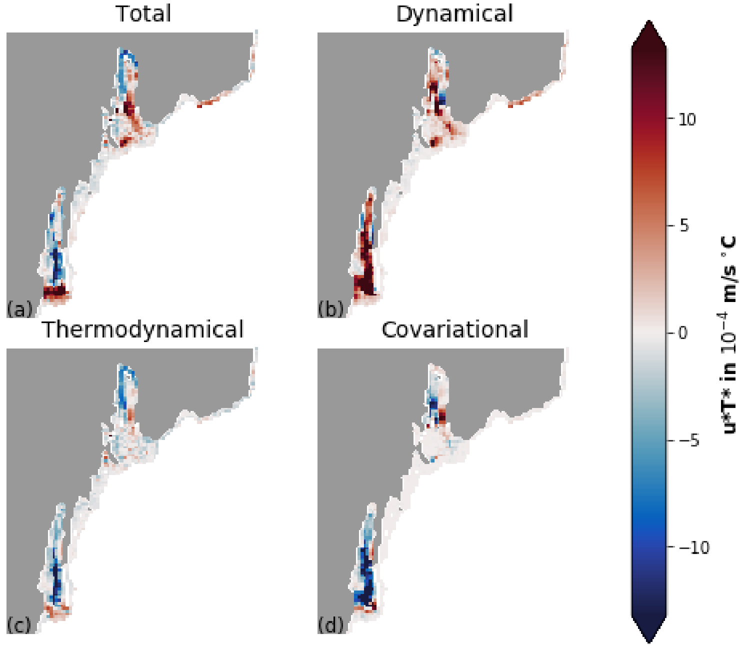

Figure B7. Same as Fig. B1, but for the Totten-Moscow University Ice Shelf System.

Author contributions. Ole Richter conceived and designed the experiments with contributions from all co-authors. Ole Richter performed the simulations. Ole Richter, David E. Gwyther and Benjamin K. Galton-Fenzi analysed the data, whereby David E. Gwyther also contributed analysis tools. Ole Richter prepared the manuscript with contributions from all co-authors.

Competing interests. The authors declare that they have no conflict of interest.

Acknowledgements. This research was supported by scholarships from the Australian Government and the Australian Research Council's Special Research Initiative for the Antarctic Gateway Partnership SRI40300001. Computational resources were provided by the NCI National Facility at the Australian National University, through awards under the Merit Allocation Scheme. We would like to thank Richard Coleman for his valuable comments on the manuscript and Just Berkhout for his excellent IT support.

References

Arzeno, I. B., Beardsley, R. C., Limeburner, R., Owens, B., Padman, L., Springer, S. R., Stewart, C. L., and Williams, M. J. M.: Ocean variability contributing to basal melt rate near the ice front of Ross Ice Shelf, Antarctica, Journal of Geophysical Research: Oceans, 119, 4214–4233, https://doi.org/10.1002/2014JC009792, https://agupubs.onlinelibrary.wiley.com/doi/abs/10.1002/2014JC009792, 2014.

Asay-Davis, X. S., Cornford, S. L., Durand, G., Galton-Fenzi, B. K., Gladstone, R. M., Gudmundsson, G. H., Hattermann, T., Holland, D. M., Holland, D., Holland, P. R., Martin, D. F., Mathiot, P., Pattyn, F., and Seroussi, H.: Experimental design for three interrelated marine ice sheet and ocean model intercomparison projects: MISMIP v. 3 (MISMIP +), ISOMIP v. 2 (ISOMIP +) and MISOMIP v. 1 (MISOMIP1), Geoscientific Model Development, 9, 2471–2497, https://doi.org/https://doi.org/10.5194/gmd-9-2471-2016, https://www.geosci-model-dev.net/9/2471/2016/, publisher: Copernicus GmbH, 2016.

Asay-Davis, X. S., Jourdain, N. C., and Nakayama, Y.: Developments in Simulating and Parameterizing Interactions Between the Southern Ocean and the Antarctic Ice Sheet, Current Climate Change Reports, 3, 316–329, https://doi.org/10.1007/s40641-017-0071-0, https://link.springer.com/article/10.1007/s40641-017-0071-0, 2017.

Bronselaer, B., Winton, M., Griffies, S. M., Hurlin, W. J., Rodgers, K. B., Sergienko, O. V., Stouffer, R. J., and Russell, J. L.: Change in future climate due to Antarctic meltwater, Nature, 564, 53, https://doi.org/10.1038/s41586-018-0712-z, https://www.nature.com/articles/s41586-018-0712-z, 2018.

Cougnon, E. A., Galton-Fenzi, B. K., Meijers, A. J. S., and Legrésy, B.: Modeling interannual dense shelf water export in the region of the Mertz Glacier Tongue (1992–2007), Journal of Geophysical Research: Oceans, 118, 5858–5872, https://doi.org/10.1002/2013JC008790, https://agupubs.onlinelibrary.wiley.com/doi/abs/10.1002/2013JC008790, 2013.

Dee, D. P., Uppala, S. M., Simmons, A. J., Berrisford, P., Poli, P., Kobayashi, S., Andrae, U., Balmaseda, M. A., Balsamo, G., Bauer, P., Bechtold, P., Beljaars, A. C. M., Berg, L. v. d., Bidlot, J., Bormann, N., Delsol, C., Dragani, R., Fuentes, M., Geer, A. J., Haimberger, L., Healy, S. B., Hersbach, H., Hólm, E. V., Isaksen, L., Kållberg, P., Köhler, M., Matricardi, M., McNally, A. P., Monge-Sanz, B. M., Morcrette, J.-J., Park, B.-K., Peubey, C., Rosnay, P. d., Tavolato, C., Thépaut, J.-N., and Vitart, F.: The ERA-Interim reanalysis: configuration and performance of the data assimilation system, Quarterly Journal of the Royal Meteorological Society, 137, 553–597, https://doi.org/10.1002/qj.828, https://rmets.onlinelibrary.wiley.com/doi/abs/10.1002/qj.828, 2011.

Egbert, G. D. and Erofeeva, S. Y.: Efficient Inverse Modeling of Barotropic Ocean Tides, Journal of Atmospheric and Oceanic Technology, 19, 183–204, https://doi.org/10.1175/1520-0426(2002)019<0183:EIMOBO>2.0.CO;2, https://journals.ametsoc.org/doi/full/10.1175/1520-0426%282002%29019%3C0183%3AEIMOBO%3E2.0.CO%3B2, 2002.

Foldvik, A., Gammelsrød, T., Slotsvik, N., and Tørresen, T.: Oceanographic conditions on the Weddell Sea Shelf during the German Antarctic Expedition 1979/80, Polar Research, 3, 209–226, https://doi.org/10.3402/polar.v3i2.6953, https://polarresearch.net/index.php/polar/article/view/2526, 1985.

Foldvik, A., Middleton, J. H., and Foster, T. D.: The tides of the southern Weddell Sea, Deep Sea Research Part A. Oceanographic Research Papers, 37, 1345–1362, https://doi.org/10.1016/0198-0149(90)90047-Y, http://www.sciencedirect.com/science/article/pii/019801499090047Y, 1990.

Fretwell, P., Pritchard, H. D., Vaughan, D. G., Bamber, J. L., Barrand, N. E., Bell, R., Bianchi, C., Bingham, R. G., Blankenship, D. D., Casassa, G., Catania, G., Callens, D., Conway, H., Cook, A. J., Corr, H. F. J., Damaske, D., Damm, V., Ferraccioli, F., Forsberg, R., Fujita, S., Gim, Y., Gogineni, P., Griggs, J. A., Hindmarsh, R. C. A., Holmlund, P., Holt, J. W., Jacobel, R. W., Jenkins, A., Jokat, W., Jordan, T., King, E. C., Kohler, J., Krabill, W., Riger-Kusk, M., Langley, K. A., Leitchenkov, G., Leuschen, C., Luyendyk, B. P., Matsuoka, K., Mouginot, J., Nitsche, F. O., Nogi, Y., Nost, O. A., Popov, S. V., Rignot, E., Rippin, D. M., Rivera, A., Roberts, J., Ross, N., Siegert, M. J., Smith, A. M., Steinhage, D., Studinger, M., Sun, B., Tinto, B. K., Welch, B. C., Wilson, D., Young, D. A., Xiangbin, C., and Zirizzotti, A.: Bedmap2: improved ice bed, surface and thickness datasets for Antarctica, The Cryosphere, 7, 375–393, https://doi.org/https://doi.org/10.5194/tc-7-375-2013, https://www.the-cryosphere.net/7/375/2013/, 2013.

Galton-Fenzi, B. K., Maraldi, C., Coleman, R., and Hunter, J.: The cavity under the Amery Ice Shelf, East Antarctica, Journal of Glaciology, 54, 881–887, https://doi.org/10.3189/002214308787779898, https://www.cambridge.org/core/journals/journal-of-glaciology/article/cavity-under-the-amery-ice-shelf-east-antarctica/D4F660A6EFACBB9047540B63190B3D57, 2008.

Galton-Fenzi, B. K., Hunter, J. R., Coleman, R., Marsland, S. J., and Warner, R. C.: Modeling the basal melting and marine ice accretion of the Amery Ice Shelf, Journal of Geophysical Research: Oceans, 117, https://doi.org/10.1029/2012JC008214, https://agupubs.onlinelibrary.wiley.com/doi/abs/10.1029/2012JC008214, 2012.

Gammelsrod, T. and Slotsvik, N.: Hydrographic and Current Measurements in the Southern Weddell Sea 1979/80, Polarforschung, https://epic.awi.de/id/eprint/28128/, 1981.

Griffiths, S. D. and Peltier, W. R.: Modeling of Polar Ocean Tides at the Last Glacial Maximum: Amplification, Sensitivity, and Climatological Implications, Journal of Climate, 22, 2905–2924, https://doi.org/10.1175/2008JCLI2540.1, https://journals.ametsoc.org/doi/abs/10.1175/2008JCLI2540.1, 2009.

Gudmundsson, G. H.: Ice-shelf buttressing and the stability of marine ice sheets, The Cryosphere, 7, 647–655, https://doi.org/https://doi.org/10.5194/tc-7-647-2013, https://www.the-cryosphere.net/7/647/2013/, 2013.

Gwyther, D. E., Galton-Fenzi, B. K., Hunter, J. R., and Roberts, J. L.: Simulated melt rates for the Totten and Dalton ice shelves, Ocean Science, 10, 267–279, https://doi.org/https://doi.org/10.5194/os-10-267-2014, https://www.ocean-sci.net/10/267/2014/, 2014.

Gwyther, D. E., Cougnon, E. A., Galton-Fenzi, B. K., Roberts, J. L., Hunter, J. R., and Dinniman, M. S.: Modelling the response of ice shelf basal melting to different ocean cavity environmental regimes, Annals of Glaciology, 57, 131–141, https://doi.org/10.1017/aog.2016.31, https://www.cambridge.org/core/product/identifier/S0260305516000318/type/journal_article, 2016.

Haney, R. L.: On the Pressure Gradient Force over Steep Topography in Sigma Coordinate Ocean Models, Journal of Physical Oceanography, 21, 610–619, https://doi.org/10.1175/1520-0485(1991)021<0610:OTPGFO>2.0.CO;2, https://journals.ametsoc.org/view/journals/phoc/21/4/1520-0485_1991_021_0610_otpgfo_2_0_co_2.xml, publisher: American Meteorological Society Section: Journal of Physical Oceanography, 1991.

Hattermann, T., Smedsrud, L. H., Nøst, O. A., Lilly, J. M., and Galton-Fenzi, B. K.: Eddy-resolving simulations of the Fimbul Ice Shelf cavity circulation: Basal melting and exchange with open ocean, Ocean Modelling, 82, 28–44, https://doi.org/10.1016/j.ocemod.2014.07.004, http://www.sciencedirect.com/science/article/pii/S1463500314000948, 2014.

Hellmer, H. H.: Impact of Antarctic ice shelf basal melting on sea ice and deep ocean properties, Geophysical Research Letters, 31, https://doi.org/10.1029/2004GL019506, https://agupubs.onlinelibrary.wiley.com/doi/abs/10.1029/2004GL019506, 2004.

Hellmer, H. H. and Olbers, D. J.: A two-dimensional model for the thermohaline circulation under an ice shelf, Antarctic Science, 1, 325–336, https://doi.org/10.1017/S0954102089000490, https://www.cambridge.org/core/journals/antarctic-science/article/twodimensional-model-for-the-thermohaline-circulation-under-an-ice-shelf/DCB7E3D1C510375CD52CBBD6C42A3993#, 1989.

Holland, D. M. and Jenkins, A.: Modeling Thermodynamic Ice–Ocean Interactions at the Base of an Ice Shelf, Journal of Physical Oceanography, 29, 1787–1800, https://doi.org/10.1175/1520-0485(1999)029<1787:MTIOIA>2.0.CO;2, https://journals.ametsoc.org/doi/full/10.1175/1520-0485%281999%29029%3C1787%3AMTIOIA%3E2.0.CO%3B2, 1999.

Jacobs, S. S.: Bottom water production and its links with the thermohaline circulation, Antarctic Science, 16, 427–437, https://doi.org/10.1017/S095410200400224X, https://www.cambridge.org/core/journals/antarctic-science/article/bottom-water-production-and-its-links-with-the-thermohaline-circulation/9C29FAEDC0136B2C616B8E7491671916, 2004.

Jacobs, S. S., Helmer, H. H., Doake, C. S. M., Jenkins, A., and Frolich, R. M.: Melting of ice shelves and the mass balance of Antarctica, Journal of Glaciology, 38, 375–387, https://doi.org/10.3189/S0022143000002252, https://www.cambridge.org/core/journals/journal-of-glaciology/article/melting-of-ice-shelves-and-the-mass-balance-of-antarctica/B4841D1BF7AD77C197F8FDA33BE9936C, 1992.

Jenkins, A., Nicholls, K. W., and Corr, H. F. J.: Observation and Parameterization of Ablation at the Base of Ronne Ice Shelf, Antarctica, Journal of Physical Oceanography, 40, 2298–2312, https://doi.org/10.1175/2010JPO4317.1, https://journals.ametsoc.org/doi/full/10.1175/2010JPO4317.1, 2010.

Jourdain, N. C., Molines, J.-M., Le Sommer, J., Mathiot, P., Chanut, J., de Lavergne, C., and Madec, G.: Simulating or prescribing the influence of tides on the Amundsen Sea ice shelves, Ocean Modelling, 133, 44–55, https://doi.org/10.1016/j.ocemod.2018.11.001, https://linkinghub.elsevier.com/retrieve/pii/S1463500318301203, 2019.

King, M. A. and Padman, L.: Accuracy assessment of ocean tide models around Antarctica, Geophysical Research Letters, 32, https://doi.org/10.1029/2005GL023901, https://agupubs.onlinelibrary.wiley.com/doi/abs/10.1029/2005GL023901, 2005.

Lewis, E. L. and Perkin, R. G.: Ice pumps and their rates, Journal of Geophysical Research: Oceans, 91, 11 756–11 762, https://doi.org/10.1029/JC091iC10p11756, https://agupubs.onlinelibrary.wiley.com/doi/abs/10.1029/JC091iC10p11756, 1986.

Liu, Y., Moore, J. C., Cheng, X., Gladstone, R. M., Bassis, J. N., Liu, H., Wen, J., and Hui, F.: Ocean-driven thinning enhances iceberg calving and retreat of Antarctic ice shelves, Proceedings of the National Academy of Sciences, 112, 3263–3268, https://doi.org/10.1073/pnas.1415137112, http://www.pnas.org/content/112/11/3263, 2015.

Llanillo, P. J., Aiken, C. M., Cordero, R. R., Damiani, A., Sepúlveda, E., and Fernández-Gómez, B.: Oceanographic Variability induced by Tides, the Intraseasonal Cycle and Warm Subsurface Water intrusions in Maxwell Bay, King George Island (West-Antarctica), Scientific Reports, 9, 1–17, https://doi.org/10.1038/s41598-019-54875-8, https://www.nature.com/articles/s41598-019-54875-8, 2019.

Loder, J. W.: Topographic Rectification of Tidal Currents on the Sides of Georges Bank, Journal of Physical Oceanography, 10, 1399–1416, https://doi.org/10.1175/1520-0485(1980)010<1399:TROTCO>2.0.CO;2, https://journals.ametsoc.org/doi/abs/10.1175/1520-0485%281980%29010%3C1399%3ATROTCO%3E2.0.CO%3B2, 1980.

MacAyeal, D. R.: Thermohaline circulation below the Ross Ice Shelf: A consequence of tidally induced vertical mixing and basal melting, Journal of Geophysical Research: Oceans, 89, 597–606, https://doi.org/10.1029/JC089iC01p00597, https://agupubs.onlinelibrary.wiley.com/doi/abs/10.1029/JC089iC01p00597, 1984.

MacAyeal, D. R.: Tidal Rectification Below the Ross Ice Shelf, Antarctica, Oceanology of the Antarctic Continental Shelf, https://agupubs.onlinelibrary.wiley.com/doi/10.1029/AR043p0109, 1985.

Mack, S. L., Dinniman, M. S., McGillicuddy, D. J., Sedwick, P. N., and Klinck, J. M.: Dissolved iron transport pathways in the Ross Sea: Influence of tides and horizontal resolution in a regional ocean model, Journal of Marine Systems, 166, 73–86, https://doi.org/10.1016/j.jmarsys.2016.10.008, http://www.sciencedirect.com/science/article/pii/S0924796316303360, 2017.

Makinson, K. and Nicholls, K. W.: Modeling tidal currents beneath Filchner-Ronne Ice Shelf and on the adjacent continental shelf: Their effect on mixing and transport, Journal of Geophysical Research: Oceans, 104, 13 449–13 465, https://doi.org/10.1029/1999JC900008, https://agupubs.onlinelibrary.wiley.com/doi/abs/10.1029/1999JC900008, 1999.

Makinson, K., Holland, P. R., Jenkins, A., Nicholls, K. W., and Holland, D. M.: Influence of tides on melting and freezing beneath Filchner-Ronne Ice Shelf, Antarctica, Geophysical Research Letters, 38, https://doi.org/10.1029/2010GL046462, https://agupubs.onlinelibrary.wiley.com/doi/abs/10.1029/2010GL046462, 2011.

Mazloff, M. R., Heimbach, P., and Wunsch, C.: An Eddy-Permitting Southern Ocean State Estimate, Journal of Physical Oceanography, 40, 880–899, https://doi.org/10.1175/2009JPO4236.1, https://journals.ametsoc.org/doi/full/10.1175/2009JPO4236.1, 2010.

McPhee, M. G.: A time-dependent model for turbulent transfer in a stratified oceanic boundary layer, Journal of Geophysical Research: Oceans, 92, 6977–6986, https://doi.org/10.1029/JC092iC07p06977, https://agupubs.onlinelibrary.wiley.com/doi/abs/10.1029/JC092iC07p06977, 1987.

Mellor, G. L., Ezer, T., and Oey, L.-Y.: The Pressure Gradient Conundrum of Sigma Coordinate Ocean Models, Journal of Atmospheric and Oceanic Technology, 11, 1126–1134, https://doi.org/10.1175/1520-0426(1994)011<1126:TPGCOS>2.0.CO;2, https://journals.ametsoc.org/doi/10.1175/1520-0426%281994%29011%3C1126%3ATPGCOS%3E2.0.CO%3B2, 1994.

Mellor, G. L., Oey, L.-Y., and Ezer, T.: Sigma Coordinate Pressure Gradient Errors and the Seamount Problem, Journal of Atmospheric and Oceanic Technology, 15, 1122–1131, https://doi.org/10.1175/1520-0426(1998)015<1122:SCPGEA>2.0.CO;2, http://journals.ametsoc.org/doi/abs/10.1175/1520-0426%281998%29015%3C1122%3ASCPGEA%3E2.0.CO%3B2, 1998.

Menemenlis, D., Campin, J., Heimbach, P., Hill, C., Lee, T., Nguyen, A., Schodlok, M., and Zhang, H.: ECCO2: High Resolution Global Ocean and Sea Ice Data Synthesis, AGU Fall Meeting Abstracts, http://adsabs.harvard.edu/abs/2008AGUFMOS31C1292M, 2008.

Mouginot, J., Rignot, E., and Scheuchl, B.: MEaSURES Antarctic Boundaries for IPY 2007-2009 from Satellite Radar, Version 1. Shelves, http://dx.doi.org/10.5067/SEVV4MR8P1ZN., 2016.

Mueller, R. D., Padman, L., Dinniman, M. S., Erofeeva, S. Y., Fricker, H. A., and King, M. A.: Impact of tide-topography interactions on basal melting of Larsen C Ice Shelf, Antarctica, Journal of Geophysical Research: Oceans, 117, https://doi.org/10.1029/2011JC007263, https://agupubs.onlinelibrary.wiley.com/doi/abs/10.1029/2011JC007263, 2012.

Mueller, R. D., Hattermann, T., Howard, S. L., and Padman, L.: Tidal influences on a future evolution of the Filchner–Ronne Ice Shelf cavity in the Weddell Sea, Antarctica, The Cryosphere, 12, 453–476, https://doi.org/https://doi.org/10.5194/tc-12-453-2018, https://www.the-cryosphere.net/12/453/2018/, 2018.

Padman, L., Howard, S. L., and Muench, R.: Internal tide generation along the South Scotia Ridge, Deep Sea Research Part II: Topical Studies in Oceanography, 53, 157–171, https://doi.org/10.1016/j.dsr2.2005.07.011, http://www.sciencedirect.com/science/article/pii/S0967064506000130, 2006.

Padman, L., Howard, S. L., Orsi, A. H., and Muench, R. D.: Tides of the northwestern Ross Sea and their impact on dense outflows of Antarctic Bottom Water, Deep Sea Research Part II: Topical Studies in Oceanography, 56, 818–834, https://doi.org/10.1016/j.dsr2.2008.10.026, http://linkinghub.elsevier.com/retrieve/pii/S0967064508003615, 2009.

Padman, L., Siegfried, M. R., and Fricker, H. A.: Ocean Tide Influences on the Antarctic and Greenland Ice Sheets, Reviews of Geophysics, 56, 142–184, https://doi.org/10.1002/2016RG000546, https://agupubs.onlinelibrary.wiley.com/doi/abs/10.1002/2016RG000546, 2018.

Padman, L., Howard, S., and King, M. A.: Antarctic Tide Gauge Database, https://www.esr.org/data-products/antarctic_tg_database, 2020.

Pritchard, H. D., Ligtenberg, S. R. M., Fricker, H. A., Vaughan, D. G., van den Broeke, M. R., and Padman, L.: Antarctic ice-sheet loss driven by basal melting of ice shelves, Nature, 484, 502–505, https://doi.org/10.1038/nature10968, http://www.nature.com/doifinder/10.1038/nature10968, 2012.

Purkey, S. G. and Johnson, G. C.: Antarctic Bottom Water Warming and Freshening: Contributions to Sea Level Rise, Ocean Freshwater Budgets, and Global Heat Gain, Journal of Climate, 26, 6105–6122, https://doi.org/10.1175/JCLI-D-12-00834.1, https://journals.ametsoc.org/doi/10.1175/JCLI-D-12-00834.1, 2013.

Reese, R., Gudmundsson, G. H., Levermann, A., and Winkelmann, R.: The far reach of ice-shelf thinning in Antarctica, Nature Climate Change, 8, 53–57, https://doi.org/10.1038/s41558-017-0020-x, http://www.nature.com/articles/s41558-017-0020-x, 2018.

Richter, O.: Whole Antarctic Ocean Model, https://doi.org/10.5281/ZENODO.3738985, 2020a.

Richter, O.: Post- and preprocessing tools for the ROMS Whole Antarctic Ocean Model, https://doi.org/10.5281/ZENODO.3738998, 2020b.

Richter, O., Gwyther, D. E., Galton-Fenzi, B. K., and Naughten, K. A.: The Whole Antarctic Ocean Model (WAOM v1.0): Development and Evaluation, Geoscientific Model Development Discussion, https://doi.org/10.5194/gmd-2020-164, in review, 2020.

Robertson, R.: Modeling internal tides over Fieberling Guyot: resolution, parameterization, performance, Ocean Dynamics, 56, 430–444, https://doi.org/10.1007/s10236-006-0062-5, https://doi.org/10.1007/s10236-006-0062-5, 2006.

Robertson, R.: Tidally induced increases in melting of Amundsen Sea ice shelves, Journal of Geophysical Research: Oceans, 118, 3138–3145, https://doi.org/10.1002/jgrc.20236, https://agupubs.onlinelibrary.wiley.com/doi/abs/10.1002/jgrc.20236, 2013.

Robertson, R. and Dong, C.: An evaluation of the performance of vertical mixing parameterizations for tidal mixing in the Regional Ocean Modeling System (ROMS), Geoscience Letters, 6, 15, https://doi.org/10.1186/s40562-019-0146-y, https://doi.org/10.1186/s40562-019-0146-y, 2019.

Rosier, S. H. R., Green, J. a. M., Scourse, J. D., and Winkelmann, R.: Modeling Antarctic tides in response to ice shelf thinning and retreat, Journal of Geophysical Research: Oceans, 119, 87–97, https://doi.org/10.1002/2013JC009240, https://agupubs.onlinelibrary.wiley.com/doi/abs/10.1002/2013JC009240, 2014.

Savage, A. C., Arbic, B. K., Alford, M. H., Ansong, J. K., Farrar, J. T., Menemenlis, D., O'Rourke, A. K., Richman, J. G., Shriver, J. F., Voet, G., Wallcraft, A. J., and Zamudio, L.: Spectral decomposition of internal gravity wave sea surface height in global models, Journal of Geophysical Research: Oceans, 122, 7803–7821, https://doi.org/10.1002/2017JC013009, https://agupubs.onlinelibrary.wiley.com/doi/abs/10.1002/2017JC013009, 2017.

Schnaase, F. and Timmermann, R.: Representation of shallow grounding zones in an ice shelf-ocean model with terrain-following coordinates, Ocean Modelling, 144, 101 487, https://doi.org/10.1016/j.ocemod.2019.101487, http://www.sciencedirect.com/science/article/pii/S1463500318302956, 2019.

Shchepetkin, A. F. and McWilliams, J. C.: The regional oceanic modeling system (ROMS): a split-explicit, free-surface, topography-following-coordinate oceanic model, Ocean Modelling, 9, 347–404, https://doi.org/10.1016/j.ocemod.2004.08.002, http://adsabs.harvard.edu/abs/2005OcMod...9..347S, 2005.

Silvano, A., Rintoul, S. R., Peña-Molino, B., Hobbs, W. R., Wijk, E. v., Aoki, S., Tamura, T., and Williams, G. D.: Freshening by glacial meltwater enhances melting of ice shelves and reduces formation of Antarctic Bottom Water, Science Advances, 4, eaap9467, https://doi.org/10.1126/sciadv.aap9467, http://advances.sciencemag.org/content/4/4/eaap9467, 2018.

Stewart, A. L., Klocker, A., and Menemenlis, D.: Circum-Antarctic Shoreward Heat Transport Derived From an Eddy- and Tide-Resolving Simulation, Geophysical Research Letters, 45, 834–845, https://doi.org/10.1002/2017GL075677, https://agupubs.onlinelibrary.wiley.com/doi/abs/10.1002/2017GL075677, 2018.

Stewart, C. L., Christoffersen, P., Nicholls, K. W., Williams, M. J. M., and Dowdeswell, J. A.: Basal melting of Ross Ice Shelf from solar heat absorption in an ice-front polynya, Nature Geoscience, p. 1, https://www.nature.com/articles/s41561-019-0356-0, 2019.

Tamura, T., Ohshima, K. I., Nihashi, S., and Hasumi, H.: Estimation of Surface Heat/Salt Fluxes Associated with Sea Ice Growth/Melt in the Southern Ocean, SOLA, 7, 17–20, https://doi.org/10.2151/sola.2011-005, https://www.jstage.jst.go.jp/article/sola/7/0/7_0_17/_article, 2011.

Timmermann, R., Wang, Q., and Hellmer, H. H.: Ice shelf basal melting in a global finite-element sea ice/ice shelf/ocean model, Annals of Glaciology, 53, https://doi.org/10.3189/2012AoG60A156, http://www.igsoc.org/annals/53/60/t60A156.html, 2012.

Turner, J., Orr, A., Gudmundsson, G. H., Jenkins, A., Bingham, R. G., Hillenbrand, C.-D., and Bracegirdle, T. J.: Atmosphere-ocean-ice interactions in the Amundsen Sea Embayment, West Antarctica, Reviews of Geophysics, 55, 235–276, https://doi.org/10.1002/2016RG000532, https://agupubs.onlinelibrary.wiley.com/doi/abs/10.1002/2016RG000532, 2017.

Williams, G. D., Herraiz-Borreguero, L., Roquet, F., Tamura, T., Ohshima, K. I., Fukamachi, Y., Fraser, A. D., Gao, L., Chen, H., McMahon, C. R., Harcourt, R., and Hindell, M.: The suppression of Antarctic bottom water formation by melting ice shelves in Prydz Bay, Nature Communications, 7, 12 577, https://doi.org/10.1038/ncomms12577, https://www.nature.com/articles/ncomms12577, 2016.

Wilmes, S.-B. and Green, J. a. M.: The evolution of tides and tidal dissipation over the past 21,000 years, Journal of Geophysical Research: Oceans, 119, 4083–4100, https://doi.org/10.1002/2013JC009605, https://agupubs.onlinelibrary.wiley.com/doi/abs/10.1002/2013JC009605, 2014.